Ann. Geophys., 27, 3645–3662, 2009
www.ann-geophys.net/27/3645/2009/

Annales Geophysicae

Climatology of planetary wave type oscillations with periods of 2–20 days derived from O_2 atmospheric and OH(6-2) airglow observations at mid-latitude with SATI

M. J. López-González[1], E. Rodríguez[1], M. García-Comas[1], V. Costa[1], M. G. Shepherd[2], G. G. Shepherd[2], V. M. Aushev[3], and S. Sargoytchev[2]

[1]Instituto de Astrofísica de Andalucía, CSIC, P.O. Box 3004, 18080 Granada, Spain
[2]Centre for Research in Earth and Space Science, York University, 4700 Keele St., Toronto, Ontario M3J 1P3, Canada
[3]Department Institute of Ionosphere, National Centre of Space Research and Technology, National Space Agency, 050020, Almaty, Kazakhstan

Received: 8 January 2009 – Revised: 3 September 2009 – Accepted: 9 September 2009 – Published: 30 September 2009

Abstract. The presence of planetary wave type oscillations at mid-latitudes in the mesosphere/lower thermosphere region has been investigated using airglow observations. The observations were taken with a Spectral Airglow Temperature Imager (SATI) installed at Sierra Nevada Observatory (37.06° N, 3.38° W) at 2900 m height. Airglow data of the column emission rate of the O_2 Atmospheric (0-1) band and of the OH Meinel (6-2) band and deduced rotational temperatures from 1998 to 2007 have been used in this study. From these observations a climatology of planetary wave type oscillations at this location is inferred. It has been found that the planetary wave type oscillations of 5-day period is predominant in our data throughout the year, with activity greater than 50% during March/April and October/November months. The planetary wave type oscillations of 2-day period is predominant during both solstices, being predominant during winter solstice in O_2 while a 10-day oscillation appears throughout the year with activity around 20% and with maximum activity during spring and autumn equinoxes. The 16-day oscillation has maximum occurrence during autumn-winter while its activity is almost disappeared during spring-summer. No clear seasonal dependence of the amplitude of the planetary wave type oscillations was observed in the cases considered in this study.

The waves simultaneously detected in the rotational temperatures deduced from both OH and O_2 emissions usually show an upward energy propagation and are affected by dissipation processes.

Keywords. Atmospheric composition and structure (Airglow and aurora; Pressure, density, and temperature) – Meteorology and atmospheric dynamics (Waves and tides)

1 Introduction

Planetary waves (PW) are planetary scale oscillations with long periods (time scale of the order of days) propagating along the longitudinal direction. They are presumed to originate in the troposphere and stratosphere by topographic forcing, land-sea heating contrast and large scale weather disturbance. Their restoring force is the variation of the Coriolis force with latitude. Planetary waves redistribute the energy, momentum and the atmospheric constituent concentrations across long distances (thousands of kilometers) (Holton, 1972). The presence of travelling planetary waves in the mesosphere and the lower thermosphere region (MLT) is well established (Vincent, 1990; Forbes and Groves, 1990; Forbes et al., 1995). These long period wave oscillations have been identified as normal modes of the atmosphere. These modes have phase speeds that are slow enough so that the period and structure (horizontal and vertical) of the mode are sensitive to the background wind system (Salby, 1981).

All planetary waves are quasi-periodic with the exact period varying within a range. The global oscillations known as 5-day, 10-day and 16-day waves are referred to as Rossby normal modes and correspond to westward propagation with

Correspondence to:
M. J. López-González
(mariajose@iaa.es)

Published by Copernicus Publications on behalf of the European Geosciences Union.

zonal number one. The vertical propagation of these waves is dependent on the mean zonal wind profile with more upward propagation during moderate westerly winds.

The quasi 2-day wave is associated with the mixed Rossby-gravity mode with zonal number of 3. In contrast to the other planetary waves the quasi 2-day wave is considered as an in-situ effect of the mesosphere. Two mechanisms have been discussed about its origin: a resonant amplification of the antisymetric (3-3) normal mode, or baroclinic instability near the summer stratospheric wind jet.

There is an enormous body of ground-based observations of the mesosphere and lower thermosphere that have been used to study the planetary wave behaviour at different latitudes: radar measurements of neutral winds (Manson et al., 2004; Vincent, 1990; Williams and Avery, 1992; Meek et al., 1996; Thayaparan et al., 1997; Jacobi et al., 1998), measurements of airglow data (Sivjee et al., 1994; Espy et al., 1997; Takahashi et al., 2002; Buriti et al., 2005; López-González et al., 2007), measurements of electron density and other ionospheric parameters of the lower and upper ionosphere (Pancheva et al., 1994, 2006; Lastovicka, 1997; Lastovicka et al., 2003; Altadill and Apostolov, 2003; Xiong et al., 2006) to mention a few. Also satellite measurements have been used to obtain the climatology of PW (Wu et al., 1994; Hirooka, 2000; Riggin et al., 2006). All these studies and observations have shown large variability in the PW activity as a function of season and latitude.

Here, the occurrence of planetary wave type oscillation in the range of 2–20 days from long term ground-based airglow observations at 37° N latitude is analysed. These observations have been made by a Spectral Airglow Temperature Imager (SATI) instrument placed at the Sierra Nevada Observatory. The instrument is capable of measuring the column emission rate and vertically averaged rotational temperature of both the O_2 Atmospheric (0-1) band, and the OH Meinel (6-2) band, using the technique of interference filter spectral imaging with a cooled CCD detector (Wiens et al., 1997). The data analysed cover the period from 1998 to 2007. A climatology of the PW activity in these airglow emission rates and in the temperature at this location is presented and the characteristics of the planetary wave type oscillations are studied.

2 Observations and method of data analysis

SATI is a spatial and spectral imaging Fabry-Perot spectrometer in which the etalon is a narrow band interference filter and the detector is a CCD camera. The SATI instrumental concept and optical configuration is described in detail by Sargoytchev et al. (2004). The instrument uses two interference filters, one centred at 867.689 nm (in the spectral region of the O_2 Atmospheric (0-1) band) and the second one centred at 836.813 nm (in the spectral region of the OH Meinel (6-2) band).

Table 1. Statistics of SATI observations.

Year	J	F	M	A	M	J	J	A	S	O	N	D
1998										23	20	10
1999		17	14	9	5	5	15	5		10	10	10
2000		16	14	8				22	10	16		
2001	5		14	11	14	8	5	6	13	18		6
2002	13	16	9			19	22	20	19	10	13	15
2005										17	21	12
2006	10	16	18	9	7	20	19	9	19	14	13	9
2007	16		15	17	19	22	23		15	18	17	
n.total	4	4	6	5	4	5	5	5	5	8	6	6

SATI measurements at 37° N have shown the presence of a clear annual variability in OH rotational temperatures while an annual modulation together with a semiannual modulation is found in O_2 rotational temperatures. Both semiannual and annual modulations have been clearly identified in both emission rates (see López-González et al., 2004, for a detailed discussion).

In the current study data from October 1998 to November 2007 have been analysed in order to derive the presence of long period oscillations in SATI measurements.

The Lomb-Scargle periodogram method (Scargle, 1982) was applied to time series formed by the whole set of data available during a single month and time series formed by all the measurements available for two consecutive months. A brief introduction to the periodogram, its normalization and the statistical significance test for the possible signals detected is provided in the Appendix.

The dataset of airglow measurements analysed in this work are composed by measurements taken continuously every 5 min during the no-moon period of each night (producing periodic gaps at 1 day intervals and gaps related to the 29-day lunar cycle). There are other additional and irregular gaps due to bad weather conditions or related to some other technical problems. Table 1 gives the number of days for each month from 1998 to 2007 with available measurements. The observation period during the night ranges from 7–8 h in June to 12–13 h in December.

The main difficulties in identifying statistically significant signals associated with planetary wave type oscillations are related to the characteristics of the SATI dataset and to the nature of the planetary wave oscillations:

1) The presence of regular gaps in the data series is common to many geophysical and astronomical measurements because of limitations in the measuring techniques where observations can only be undertaken at night. Hernandez (1999) pointed out how the presence of regular gaps in the time series produces power peaks corresponding to false signals in the periodograms together the power peak corresponding to the true signals. These false peaks signals could mask the presence of the true signals present in the data series. Gaps in the observational data series at regular

frequency w_g could introduce false peaks w_f which are ghost images of the real peaks w_s. The false peaks are strongest at frequencies $w_f = w_s \pm k w_g$ and k is an integer.

Normally, except for the observational 1 day gap, the gaps are irregularly spaced in the time series of SATI measurements, and then the false peaks have small power, but special care has to be taken with possible false peaks when the gaps have some regularity (see Appendix).

The periodograms applied to time series of a month of data show significant power peaks in the region of period shorter than about 1 day. These significant peaks are found at periods of about 1 day, half day and possibly one third part of a day. Together these significant peaks corresponding to tide type oscillations may be identified other significant peaks related to true longer period oscillations and the 1 day gap present in the time series.

Figure 1 shows a time series of data corresponding to October 2007. The periodograms for these time series show significant peaks at periods about 7 days (w_s=0.14d^{-1}) in both temperatures and in the O_2 emission rates. There are also other peaks at 1.17 and 0.875 days (w_s-1 and w_s+1) that are false peaks. These false peaks disappear when a periodic signal of period 7 days with the amplitude and phase obtained by a least squares procedure is subtracted from the time series. Figure 1 also shows the periodograms obtained for the time series of O_2 emission rates and both temperatures after subtracting the corresponding 7 days periodic signals. There remain the peaks at periods of 0.5, 1 and 0.33 days. The semidiurnal tide (0.5 days period or w_s=2d^{-1}) seems the predominant tide oscillation while the peaks at 1 and 0.33 days (w_s-1 and w_s+1), corresponding to possible diurnal and terdiurnal tide, disappear after subtracting from the data series the periodic oscillation of period of 0.5 days. Other modulations of short periods (about hours) that could be present during individual nights cannot be identified in the periodograms above a solid level of significance. The diurnal and semidiurnal tides have been studied in SATI data by López-González et al. (2005). A distinct seasonal behaviour in the tidal variations was found in SATI data: a mainly semidiurnal tidal variations in both rotational temperatures and emission rates throughout the entire year except during early spring when the tidal variations seem to be consistent with a diurnal modulation.

In the present work true signals with periods in the range from 1.4 to 20 days are investigated. Periods longer than 20 days, that could be associated with the orbital period of the Moon or to the rotation period of the Sun or other longer period planetary wave type oscillations, are not analysed in the present study. The possible true signals of period greater than 1.4 days and the 1 day gap present in the time series analysed may produce false signals identifications at periods shorter than 3 days. Although the periodograms obtained from nightly averaged data and those obtained from all the nightly data measured every 5 min are very similar a clear tendency to reduce the false peaks in the region around the

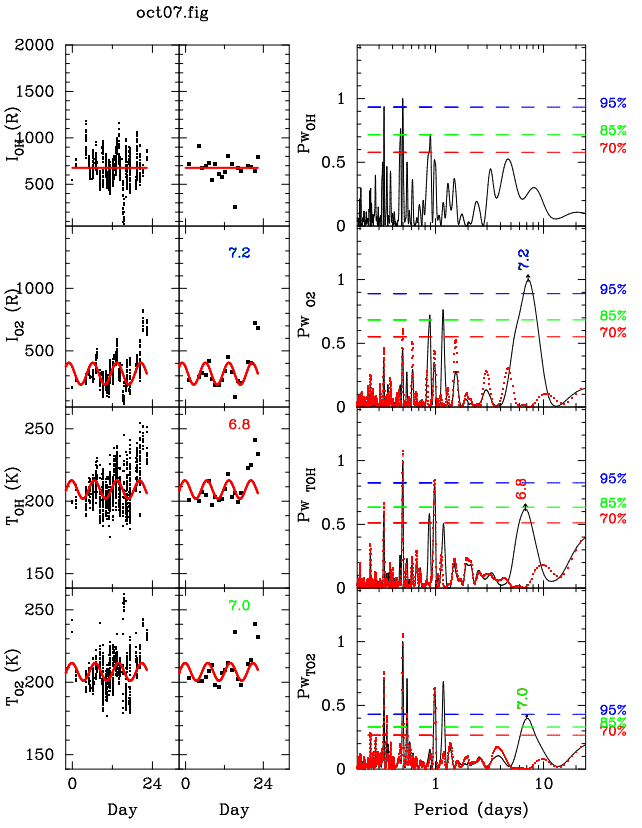

Fig. 1. Emission rates and rotational temperatures during October 2007. Left panel: Measurements. Solid line: Numerical calculation. Middle panel: Nightly averaged measurements. Solid line: Numerical calculation. Right panel: Periodograms. Solid line: for time series measurements. Dotted and red line: for time series measurements after subtraction of the 7 day period detected signal.

2 day period is observed when all the data are used (see Appendix). The use of all nightly data make possible the detection of the true signal in this short period region by reducing the power of the false peaks.

2) The length of the time series is limited for the characteristics of these observations and for the quasi periodic nature of these atmospheric modulations.

The finite length of the time series analysed (ΔT=day $_N$−day $_1$) imposes a limit in the frequency resolution $\Delta w = \frac{1}{\Delta T}$ (or period resolution $\Delta T_p = \frac{T_p^2}{\Delta T}$) and a limitation in the level of significance required for the peaks in the periodograms to be considered as significant signals. Under good conditions the length of a time series of one month of data is around 20 days of observations per month. This produces a period resolution (width of the peaks) at periods of 2, 5, 10, and 16 days of 0.2, 1.1, 5 and 13 days, respectively. These peaks become wider as the time series become shorter, making the detection of long period signals difficult. To increase the period resolution and to detect long period signals it should be useful to analyze two consecutive

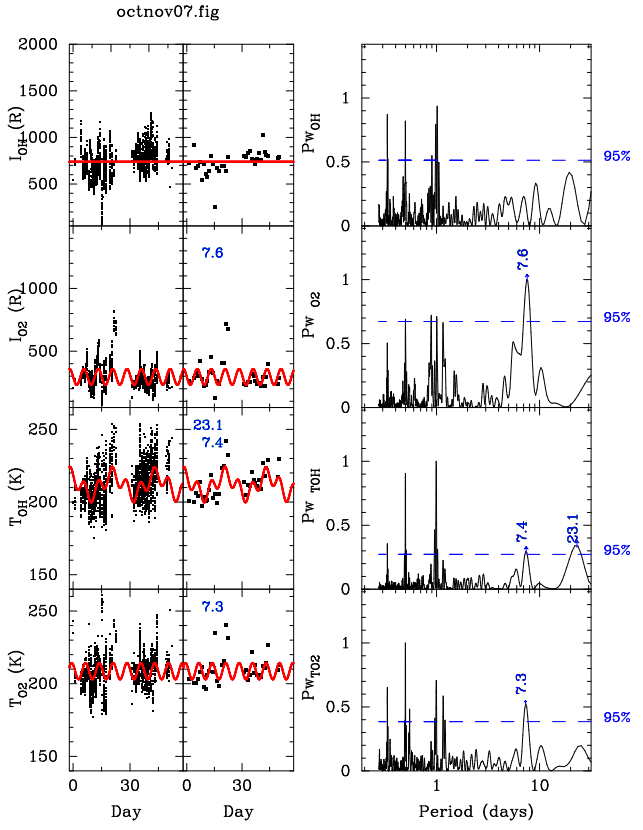

Fig. 2. As Fig. 1 but for October–November 2007.

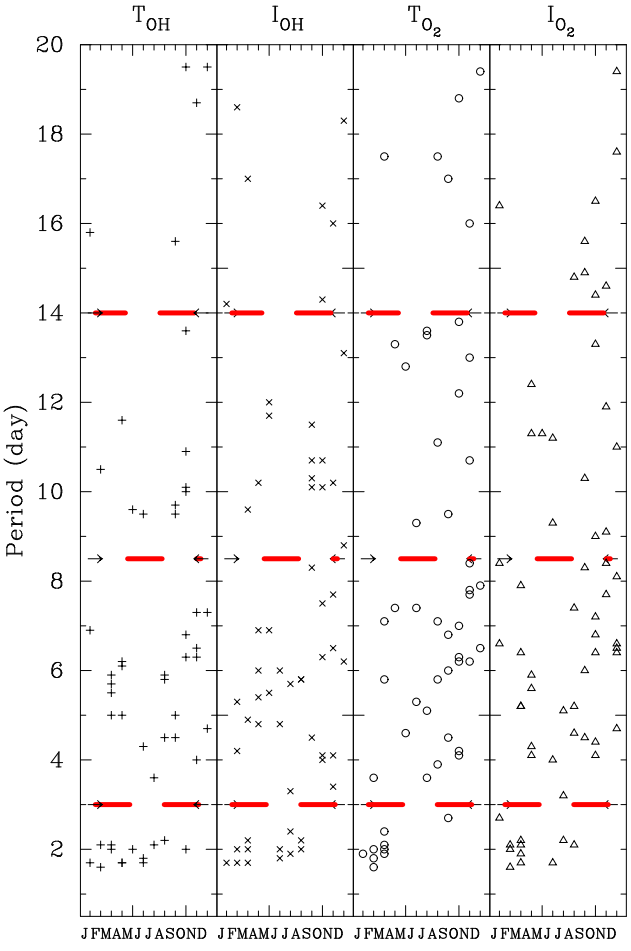

Fig. 3. Periods of possible wave oscillations detected in the whole set of measurements. Dashed lines: limits between the period regions considered.

months of data, although the additional problem of the long gap between the two months of data may introduce some additional noise and spurious peaks in the corresponding periodograms. On the other hand the quasi-wave nature of the planetary waves produces probable random fluctuations in amplitude, phase and period of these signals. Moreover a clear and detectable persistence for more than 6–8 cycles can be considered very optimistic. This quasi-wave nature of planetary waves type oscillation introduces additional noise in the data and more difficulties in the detection of these planetary wave type oscillations (see the Appendix).

Therefore in this study the Lomb-Scargle periodograms have been applied to series of a single month of data, using all nightly measurements (useful to define short period oscillations) and to series of two months of data (useful to confirm or discard long period oscillations). The analysis of time series of two months of data is specially needed in the case of months with a small number of days of available data and with possible long period oscillations. However in this case, the quasi periodic nature of the planetary wave modulations make the identification of short period modulations more difficult.

When time series of one month of data are analysed, only those peaks above a confidence level of 70% have been considered as possible oscillations present in the data. Peaks above a confidence level of 95% are considered as oscillations present in the data, when series of two consecutive months of data are analysed. These criteria have been chosen to select a sample of possible planetary wave type oscillations in SATI dataset and to study its behaviour.

Figure 1 shows the power peaks of the periodograms, above the corresponding confidence levels, following our selected criterion for the time series corresponding to October 2007. The numerical calculations of the selected oscillations are also plotted.

Figure 2 shows a time series of data corresponding to two consecutive months during 2007 (October–November of 2007). The periodograms obtained and the peaks above a confidence level greater than 95% are shown and marked. The nightly averaged data and the calculated numerical perturbation obtained by fitting the data in a least mean square sense with the periods, amplitudes and phases obtained from the Lomb-Scargle analysis of these measurements are also plotted in Figs. 1 and 2. Amplitudes and

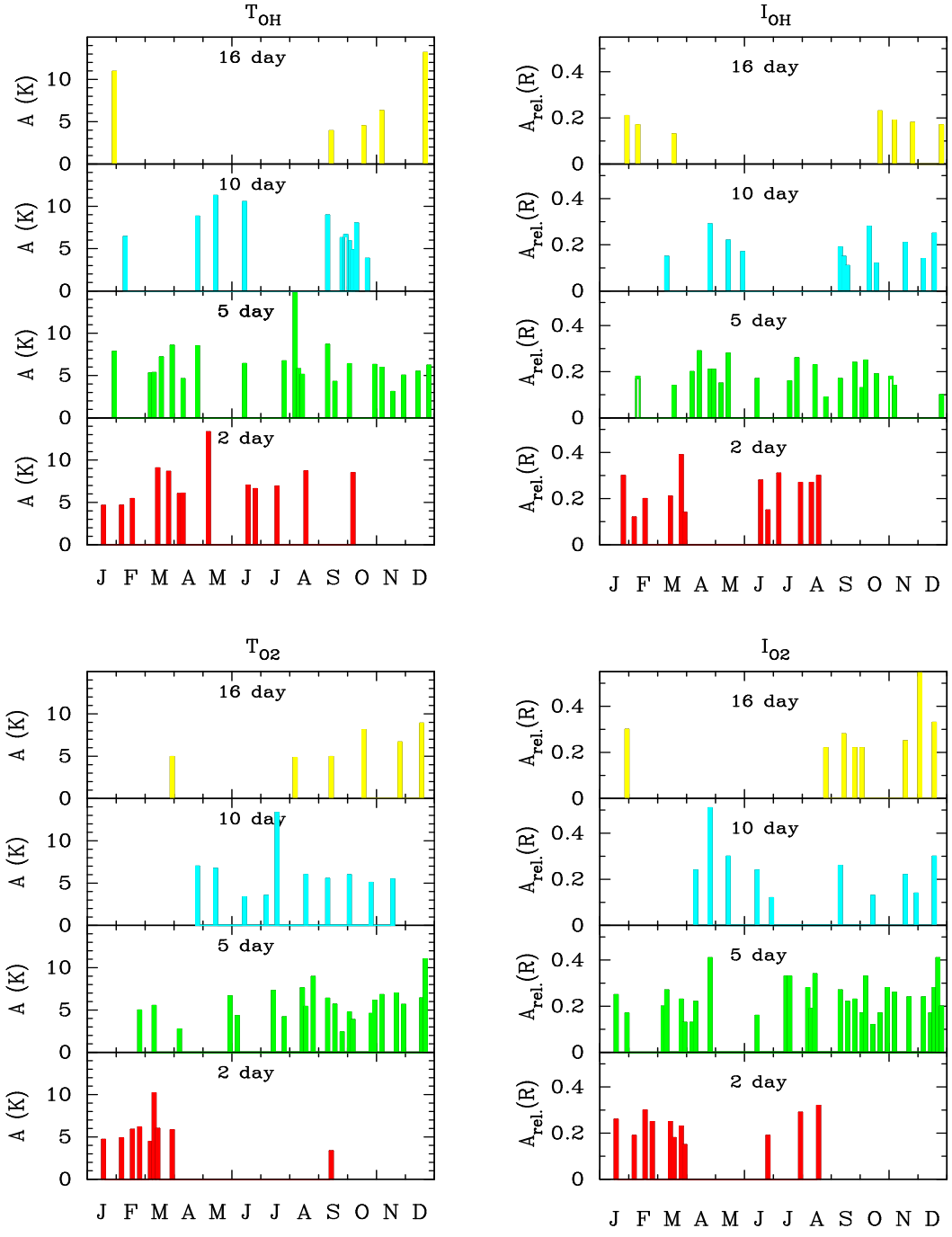

Fig. 4. Amplitudes of planetary wave type oscillations identified as function of the month.

phases corresponding to the spectral peaks identified in the periodogram are calculated simultaneously with the Lomb-Scargle periodogram method (Hocke, 1998). These amplitudes and phases obtained are equivalent to a least squares fitting of the data to a pure sinusoidal function following the relation $y(t)=A\cos((2\pi/T)t-\phi)$ where A is the amplitude, T is the period and ϕ is the phase respect to an initial time.

This approach has been applied to the available data for each month of the period of interest (1998–2007). Figure 3 shows the periods of the different oscillations detected in SATI data as a function of the month. These oscillations have been divided into four groups: 1) the 2-day group covering a range of periods from 1.4 to 3 days, 2) the 5-day group (covering a range of periods from 3 to 8.5 days), 3) the 10-day group (covering a range of periods from 8.5 to 14 days) and

4) the 16-day group (covering a range of periods from 14 to 20 days). For the OH emission rates and temperatures these groups appear clearly identified. However, for O_2 emission rates and temperatures the ranges of periods are more spread out and the range of periods are not as clearly marked except for the 2-day group, which remains clearly defined as in OH (see Fig. 3).

The behaviour of these different groups of oscillations is examined and discussed in the following sections.

3 Results

The amplitudes of the different oscillations detected in the data, corresponding to these four groups mentioned, are plotted in Fig. 4.

Although the amplitudes of the oscillations found for both temperatures and emission rates do not show strong differences it can be seen that in general the amplitudes in OH temperature oscillations are greater than those of the O_2 temperature oscillations for all groups considered while relative amplitudes in O_2 emission rate oscillations are larger than in OH emission rate oscillations. Even though there is no marked strong seasonal dependence, there is a trend towards larger amplitudes during summer (from late spring to late summer) for the 2-day, 5-day and even 10-day planetary wave type oscillations in both, OH and O_2, temperatures and emission rates. However, no dependence of the amplitude of these modulations on the wave period was found.

On the other hand, in order to study the occurrence of wave oscillations of the different groups, the probability of finding an oscillation of one of these groups for a given month has been calculated as the number of oscillations found for the corresponding month, during all years considered, averaged by the total number of the corresponding months of available data. The results are shown in Fig. 5. The 5-day oscillation is the most predominant in both temperature and emission rate datasets. The 2-day wave is a strong feature for OH temperature and emission rate from winter to summer, whereas for O_2 temperature and emission rate the 2-day wave is stronger during winter. The 10-day wave seems to be present mainly during both equinoxes while during summer and winter the 10-day wave activity is smaller. Moreover very little 16-day wave activity is detected in summer.

3.1 2-day

Maximum 2-day wave activity has been reported during solstices and minima at the equinoxes at middle and at high latitudes (Nozawa et al., 2005; Chshyolkova et al., 2005; Murphy et al., 2007; Jacobi et al., 2008).

From our measurements at 37° N the range of periods of the planetary wave-like oscillations found for this group is very well defined (see Fig. 3). A mean period of 1.9±0.2 day is found for both OH temperatures and emission rates, while a mean period of 2.1±0.4 day is found for both O_2 emission rates and temperatures. The small dispersion in the mean period indicates that the range of periods in this group is narrow and clearly marked. Amplitudes in OH temperatures are in general greater than in O_2 temperature. As seen in Fig. 5 the 2-day wave is strong in winter and summer in OH while in O_2 it is predominant in winter and almost disappears in summer. In addition, the amplitude of these oscillations in OH temperatures are usually larger in summer than in winter.

The O_2 airglow layer is formed in a two-step process, the first being the three-body recombination of atomic oxygen to form excited molecular oxygen, O_2*, and the second being the energy transfer to O_2 to form $O_2(b^1\Sigma_g^+)$. Neglecting quenching effects make the profile roughly proportional to the product of $[O]^2$ and O_2. Thus the altitude and shape of the profile are dominated by the constituent profiles of atomic and molecule oxygen with a typical peak altitude of 95 km as observed from rocket measurements by Witt et al. (1979, 1984) and Greer et al. (1986). The OH emission is produced by the reaction of ozone and atomic hydrogen, but the ozone is produced by the reaction of atomic oxygen with O_2, so that the OH emission is roughly proportional to [O], locating it below the O_2 emission normally at 87 km, as observed by rocket measurements by Baker and Stair (1988). Liu and Shepherd (2006a) have shown profiles of the $O(^1S)$, O_2 atmospheric and OH emissions obtained from the WINDII instrument on NASA's Upper Atmosphere Research satellite. These show considerable overlap, but with clearly distinct peaks. Liu and Shepherd (2006b) conducted a detailed study of the statistical distribution of OH altitudes, and found an empirical model for this, depending strongly on the emission rate, and weakly on the solar flux and the day of the year (seasonal variation). The total altitude variation at mid latitudes is about 7 km and this is attributed to planetary waves and tides. The interpretation is that the downward vertical dynamical motions of these waves brings down atomic oxygen rich air from above, increasing the emission rate and lowering the altitude while upward motions introduce atomic oxygen poor air that reduces the emission rate for higher altitude. Thus the chemistry determines the altitudes of the airglow layers relative to one another while the dynamics move all the layers up and down together.

The analysis of SATI measurements shows strong winter and summer 2-day wave activity at the altitude of the peak of the OH emission layer (around 87 km) and less 2-day wave activity during summer, while larger activity during winter is detected at altitudes of the peak of the O_2 emission layer (around 95 km). This behaviour found at 37° N agrees with the behaviour reported at middle latitudes for the 2-day wave.

3.2 5-day

The 5-day wave is the most prominent feature in our dataset. This is in agreement with the theoretical peak activity at mid-latitudes (Salby, 1981) and observations at midlatitudes

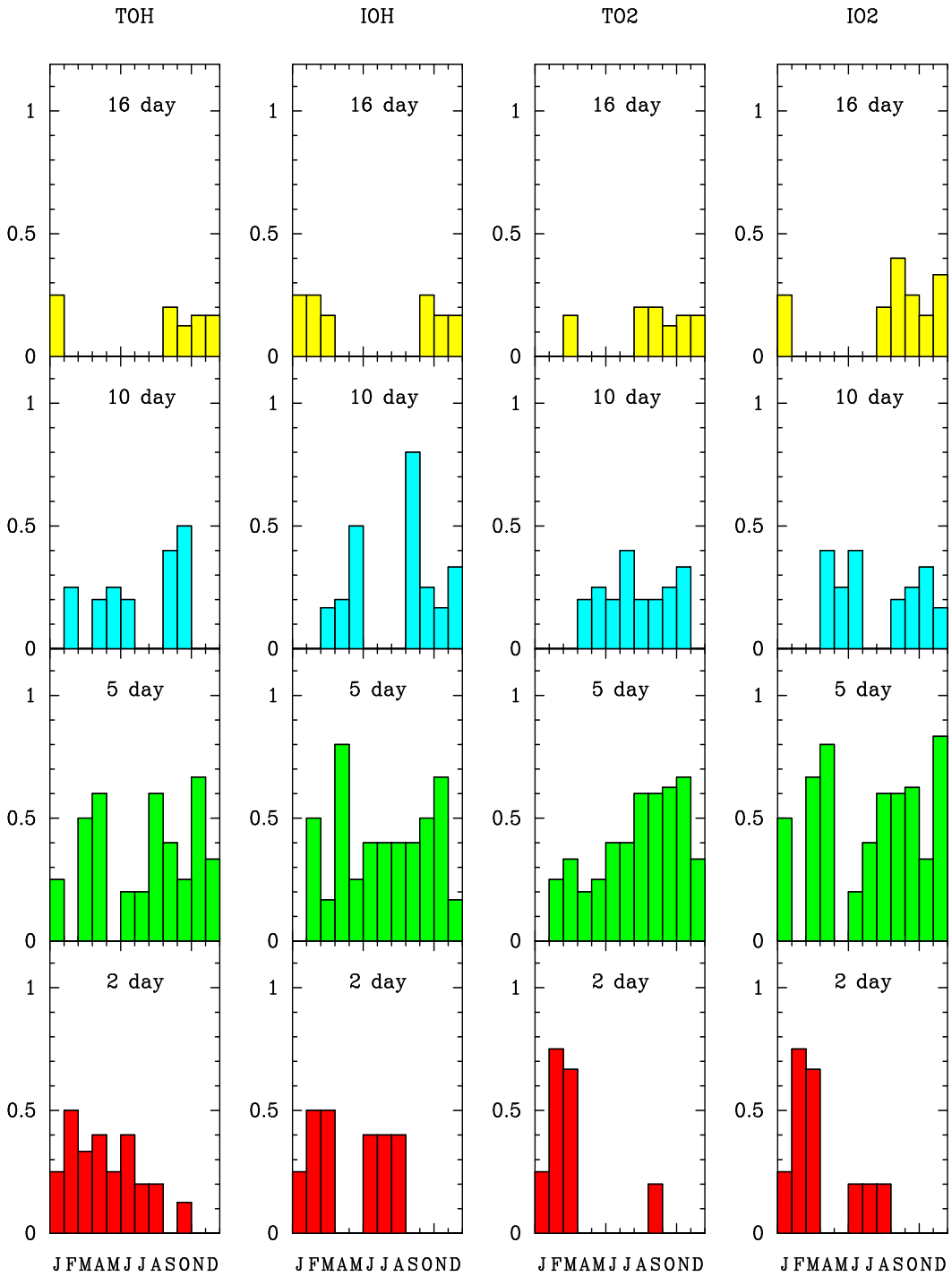

Fig. 5. Seasonal dependence of the probability of wave occurrence.

(Hirota and Hirooka, 1984; Wu et al., 1994; Yee et al., 2001; Riggin et al., 2006).

The 5-day wave appears during almost the entire year. A probability of occurrence larger than 50% is detected around March/April and October/November in agreement with the main peak of activity for the 5-day waves around April/May reported by Riggin et al. (2006) based on 3 years of SABER temperature observations.

The amplitude of the 5-day waves seems to be a little larger around late summer (August) in both temperatures and emission rates (see Fig. 4), although there is no clear seasonal dependence of the amplitudes of this type of wave.

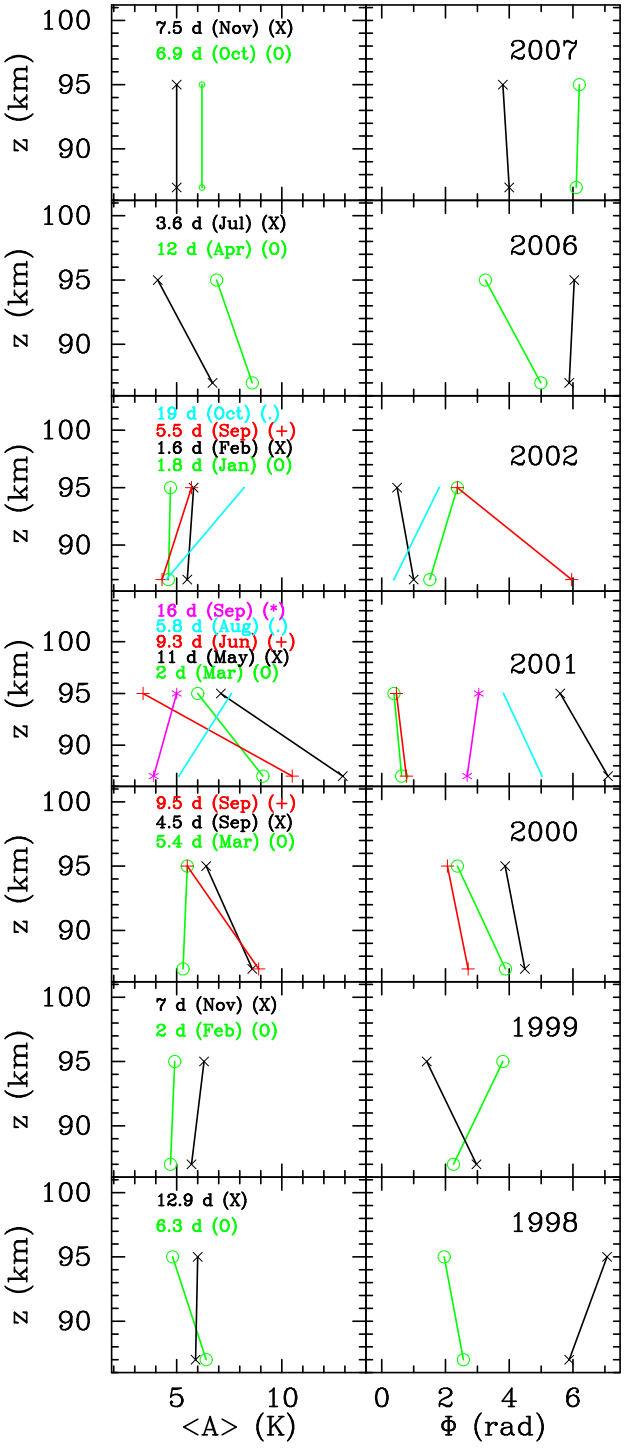

Fig. 6. Amplitudes and phases of the oscillation detected in the temperature oscillations as function of the altitude.

3.3 10-day

The maximum wave activity in this group is found during the equinox seasons, while the minimum activity is found during the solstice seasons. The autumn appears to be the period of maximal activity. The amplitudes of 10-day oscillations seem to be somewhat larger around late spring, but no seasonal dependence of the amplitudes of 10-day oscillations is found from these measurements.

This wave is not as prominent as the 5-day wave. It has a probability of occurrence of about 20%. Its behaviour at 37° N is somewhat different in comparison with that reported at higher latitudes where the 10-day and 16-day waves have been found to be stronger than the 5-day waves in winter (Lawrence and Jarvis, 2001; Manson et al., 2004, 2005).

Table 2. Wave parameters detected in temperature oscillations.

	OH			O_2				
Month	Period (day)	A (K)	Φ (rad)	Period (day)	A (K)	Φ (rad)	λ_z (km)	ΔA (K)
Oct98	6.3	6.4	2.56	6.3	4.8	1.96	83.8	−1.63
Oct98	13.6	5.9	5.88	12.2	6.0	7.07	−42.2	0.06
Feb99	2.1	4.7	2.25	2.0	4.9	3.80	−32.4	0.22
Nov99	6.5	5.7	2.97	7.7	6.3	1.41	32.2	0.57
Mar00	5.0	5.3	3.88	5.8	5.5	2.37	33.3	0.19
Sep00	4.5	8.6	4.49	4.5	6.4	3.87	81.1	−2.26
Sep00	9.5	8.9	2.71	9.5	5.5	2.06	77.3	−3.41
Mar01	2.1	9.1	0.62	1.9	6.0	0.38	201.9	−3.09
May01	9.6	12.9	7.10	12.8	7.1	5.60	33.5	−5.76
Jun01	9.5	10.5	0.77	9.1	3.4	0.46	162.1	−7.14
Aug01	5.8	5.1	5.03	5.8	7.6	3.82	41.5	2.48
Sep01	15.6	3.9	2.68	17.0	5.0	3.04	−139.6	1.04
Jan02	1.7	4.6	1.51	1.9	4.7	2.37	−58.4	0.07
Feb02	1.6	5.5	1.00	1.6	5.8	0.48	96.7	0.37
Sep02	5.0	4.3	5.96	6.0	5.7	2.37	14.0	1.39
Oct02	19.5	4.5	0.38	18.8	8.2	1.80	−35.4	3.66
Apr06	11.6	8.6	4.99	13.3	6.9	3.25	28.9	−1.72
Apr06	3.6	6.7	5.88	3.6	4.1	6.04	−314.2	−2.52
Oct07	6.8	6.2	6.10	7.0	6.2	6.20	−502.7	−0.03
Nov07	7.3	5.0	4.00	7.8	5.0	3.80	251.3	0.07

This wave is not as prominent as the 5-day wave. It has a probability of occurrence of about 20%. Its behaviour at 37° N is somewhat different in comparison with that reported at higher latitudes where the 10-day and 16-day waves have been found to be stronger than the 5-day waves in winter (Lawrence and Jarvis, 2001; Manson et al., 2004, 2005).

3.4 16-day

The amplitude of the oscillation in OH temperature is larger than in O_2 temperature. This indicates that, in general, the amplitude of oscillation in temperature decreases with altitude. A larger activity in the 16-day oscillation is found from autumn to late winter. During spring and summer this wave oscillation almost disappears. This maximum activity during winter season has been found at other middle and high latitude locations (e.g. Namboothiri et al., 2002; Manson et al., 2004, 2005; Jacobi et al., 1998, 2008; Mitchell et al., 1999; Luo et al., 2000, 2002; Jiang et al., 2005).

3.5 Vertical propagation

The measurements used in this work have been taken at one location, so no information on the horizontal (zonal or meridional) characteristics of the detected waves can be obtained. However, from our data there are cases when an oscillation is detected in the temperature deduced from both OH and O_2 emissions. When an oscillation in atmospheric temperature

at two altitude levels is observed then information about the vertical propagation of this oscillation can be inferred. In Table 2, periods, amplitudes and phases of the oscillations simultaneously detected in the temperature at these two atmospheric levels are listed. As was mentioned earlier the altitude and shape of the OH and O_2 airglow layers are not constant and the altitude of these emission layers may change by a few kilometres with respect to theirs respective "mean location" because of different dynamical processes, but the OH layer is always at a lower altitude than O_2 emission layer.

In any case these emissions give information on atmospheric layers that to some extent overlap. However the small difference in height (a few kilometres) allows important information about temperature amplitudes and phases to be obtained over a very small altitude region. Figure 6 shows the amplitudes and phases of these oscillations at the altitudes of the OH and O_2 volume emission peaks (~87 km and 95 km, respectively).

By using the phases of the waves detected in the temperature deduced from O_2 emission (at ~95 km) and deduced from OH emission (at ~87 km) the vertical wavenumber, $\nu_z = \delta\phi/\delta z$, or vertical wavelength, $\lambda_z = 2\pi/\nu_z$, can be calculated. Here, in order to make an easy numerical estimation of the vertical wavelength it is assumed that O_2 emission peak is located at 95 km and OH emission peak at 87 km. However as the vertical wavelength is proportional to the difference in the height of these airglow emissions ($\lambda_z \sim 2\pi\,\Delta z/\Delta\phi$), the closer the layers are, the shorter the wavelength will be and vice versa.

A positive slope in phase with altitude implies a downward energy propagation and a negative slope an upward energy propagation (under the assumption of the O_2 emission layer is placed higher than the OH emission layer). Table 2 gives the vertical wavelengths obtained (here a positive vertical wavelength indicates upward energy propagation, a decrease of the phase with altitude).

There are 20 cases of waves simultaneous detected in OH and O_2 temperatures. From these we have found upward energy propagation in 13 cases, and downward energy propagation in 7 cases. This result has to be considered carefully, taking into account the restriction of considering that the wave does not change with height, when in most of the cases considered the period of the waves deduced from the fitting is slightly different at these two altitudes, and this can introduce an uncertainty in the phases obtained in the process of wave fitting. However, this procedure can give us at least general and qualitative information on the vertical propagation.

Figure 7a gives the vertical wavelengths as function of the month. We see that the upward energy propagation is predominant throughout the year. There are some cases with very long wavelengths corresponding to phases very similar at the O_2 and OH emission altitudes so a small error in phase determination could produce a different sense in the direction of the vertical energy propagation and in turn an incorrect determination of the direction of the calculated vertical energy propagation. For example, October 2007 seems to be a month with downward energy propagation and very long wavelengths which only means that the phase difference of the wave at these two altitudes is very small. The number of cases with detected simultaneous oscillations in the temperature at OH and O_2 emission heights increases in September and October and together with the predominant upward energy propagation, a downward energy propagation can also be detected.

The comparison of waves detected simultaneously in these two emissions coming from two different airglow emission layers at two different altitude levels has also been used as an indicator of the direction of the vertical propagation of the corresponding detected wave.

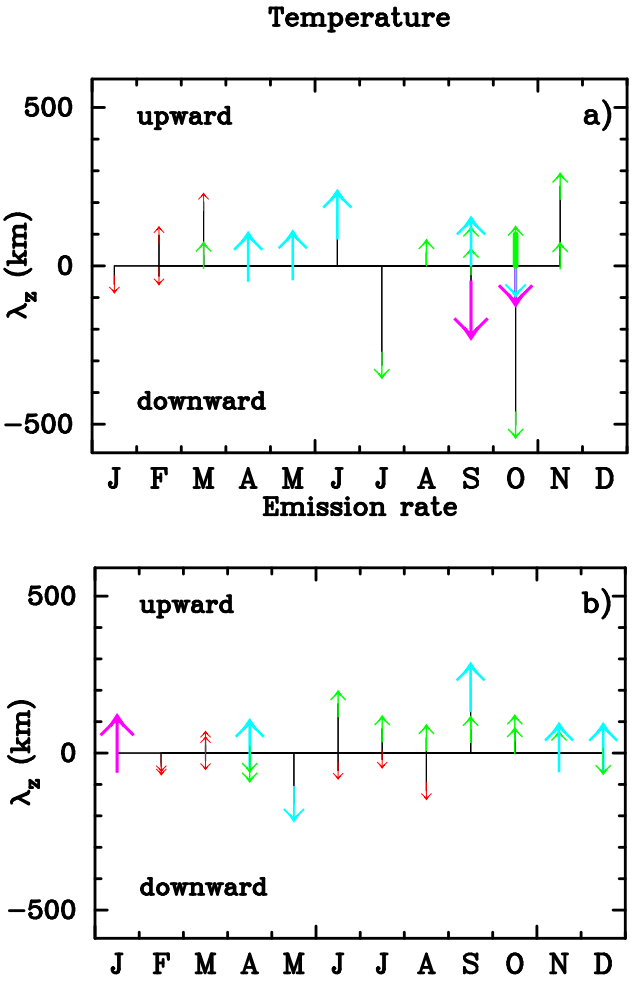

Fig. 7. Vertical wavelength as function of the month. Red and small arrow: 2-day; Green and normal arrow: 5-day; Blue and big arrow: 10-day; Pink and huge arrow: 16-day. **(a)** Calculated from temperature. **(b)** Calculated from emission rate.

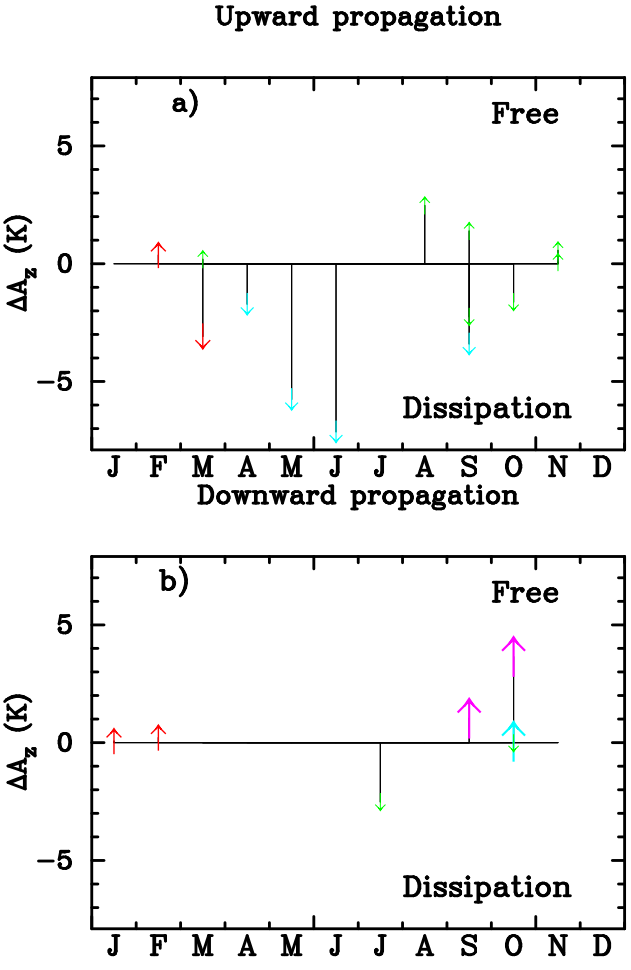

Fig. 8. Amplitude variation (difference between the amplitudes of a simultaneous oscillation detected in the temperatures deduced from both OH and O_2 emissions) as function of the month. Red and normal arrow: 2-day; Green and small arrow: 5-day; Blue and big arrow: 10-day; Pink and huge arrow: 16-day **(a)** Upward energy propagation. **(b)** Downward energy propagation.

There are 25 cases of waves simultaneously detected in OH and O_2 emission rates. Table 3 lists periods, normalized amplitudes and phases of the oscillations simultaneously detected in the two airglow emissions. Table 3 also lists the vertical wavelengths obtained for these waves and Fig. 7b shows that there are 14 cases of upward propagation and 10 cases of downward propagation while there is one case with an infinite wavelength (a phase difference less than 0.01 radians). These oscillations detected in both emission rates also indicate a slightly larger upward propagation and a possible greater activity in September–October and March–April periods. Using the results of Liu and Shepherd (2006b) and an oscillation amplitude of 20% in emission rate, the predicted total altitude change is about 1.9 km.

Table 3. Wave parameters detected in emission rate oscillations.

	OH			O_2			
Month	Period (day)	A_{rel} (R)	Φ (rad)	Period (day)	A_{rel} (R)	Φ (rad)	λ_z (km)
Oct98	6.3	0.13	3.10	6.4	0.17	1.82	39.3
Feb99	2.0	0.12	5.94	2.0	0.19	7.50	−32.2
Apr99	5.4	0.20	2.38	4.1	0.13	4.93	−19.7
Oct99	4.0	0.25	6.39	4.4	0.33	5.76	79.8
Nov99	6.5	0.14	3.65	7.7	0.26	1.86	28.1
Sep00	10.3	0.19	2.66	9.5	0.26	2.42	209.4
Sep00	4.5	0.17	4.69	4.4	0.27	4.69	inf
Mar01	1.7	0.21	1.84	1.9	0.25	0.66	42.4
May01	12.0	0.22	5.46	11.3	0.30	5.77	−162.1
Jun02	4.8	0.17	6.29	4.0	0.16	5.97	157.1
Aug02	5.8	0.23	5.47	5.2	0.34	4.45	49.3
Feb02	1.7	0.20	0.30	1.6	0.30	1.48	−42.5
Jul02	3.3	0.16	2.28	3.2	0.33	1.63	77.3
Aug02	2.2	0.30	0.64	2.1	0.32	1.06	−120.8
Nov02	10.2	0.21	7.11	11.9	0.22	4.32	18.0
Dec02	8.8	0.25	4.35	11.1	0.30	1.47	17.5
Mar06	2.0	0.39	8.04	2.1	0.23	6.02	24.9
Apr06	10.2	0.29	6.02	12.4	0.51	4.34	29.9
Apr06	6.0	0.21	1.25	5.6	0.41	2.24	−50.8
Jun06	2.0	0.15	3.94	1.7	0.19	4.84	−55.9
Sep06	8.3	0.24	3.90	8.3	0.23	3.23	75.0
Dec06	6.2	0.10	4.93	4.7	0.20	6.83	−26.5
Jan07	14.2	0.21	4.25	16.4	0.30	2.61	30.6
Mar07	2.2	0.14	4.54	1.7	0.15	6.53	−25.3
Jul07	2.4	0.27	1.94	2.2	0.29	4.39	−20.5

The wave amplitude should increase exponentially with height, to conserve the wave energy, if there were no dissipation processes. Wave amplitudes at the altitude of the O_2 emission layer (∼95 km) should be greater than at the altitude of the OH emission layer (∼87 km), if there were no dispersion, friction or dissipation. However the waves lose energy by different dissipation processes such as molecular and eddy viscosity and radiative damping in which case the wave amplitude can decrease with height. To have a qualitative estimation of the vertical propagation of the waves, the difference in the amplitudes for the waves detected in the temperature deduced from both O_2 and OH airglow emissions is considered as an indicator of the degree of freedom (amplitude increases with height) or dissipation (amplitude decreases with height) that affects the vertical propagation of the waves. Figure 8a shows the difference in the amplitudes of the waves detected in the temperature deduced from O_2 emission and OH emission, as a function of the month, for the cases in which upward energy propagation is found (see Fig. 7a). Figure 8b gives the difference in these wave amplitudes in the cases in which a downward energy propagation was obtained. A negative amplitude variation indicates that amplitude in the modulation detected in the temperature decreases with the altitude (energy decreases with height) indicating that waves are breaking or are being externally damped by eddy or molecular processes. Figure 8a shows

that in most of the cases considered the waves are affected to some degree by dissipation processes, but there are a few cases in which wave amplitude still increases with height. These cases present a propagation with greater freedom and weaker dissipation.

Figure 8b shows that the amplitude increases with height more commonly in the cases when a possible downward energy propagation is detected. For these cases the propagation appears to be qualitatively freer of dissipation.

In conclusion, the wave oscillations detected in this work show mainly upward energy propagation and the vertical propagation is affected to some degree by different dissipation processes. The waves with a downward energy propagation are not as much affected by dissipation as those propagating upward.

4 Conclusions

The activity of planetary wave type oscillations in the mesosphere and lower thermosphere has been investigated at 37.06° N using airglow measurements of OH (6-2) Meinel band and O_2 (0-1) atmospheric oxygen band emissions.

The strongest activity found with periods ranging from 2 to 20 days has been related to the 5-day wave. It appears throughout the year at both OH and O_2 altitudes. Wave activity is larger around March/April and October/November periods.

The oscillations detected in the range from 1.4 days to 3 days that could correspond to the quasi 2-day wave are also a strong feature in these data. This 2-day wave has a significant presence during winter and summer at OH altitudes with a probability of occurrence close to 30%. However at O_2 altitudes the quasi 2-day wave is mainly restricted to winter months and has stronger presence than that observed in the winter OH data.

The oscillations with periods from 8.5 days to 14 days appear throughout the year with a probability of occurrence of about 20%. The activity is more concentrated at the equinoxes.

Oscillations with periods in the range from 14 days to 20 days are the least persistent in these data. These oscillations could correspond to the quasi 16-day wave. The largest activity at Sierra Nevada site is concentrated during autumn and winter. This wave almost disappears during spring and summer.

A seasonal behaviour in the amplitudes of these wave type oscillations has not been found.

The amplitude in oscillations of the temperature at OH level are in general greater than at O_2 level. A downward phase propagation is normally found in the temperature oscillations detected simultaneously at OH and O_2 emission heights. Also a downward phase propagation is more frequently found in the waves detected simultaneously in both emission rates. In general an upward energy propagation affected by a different degree of dissipation is inferred throughout the year (from the waves observed in the temperature deduced from the O_2 and OH airglow emissions).

Appendix A

A1 The periodogram

The periodogram is an extremely valuable tool in assessing periodic signals in all types of time series. The periodogram provides a reasonable good approximation to the spectrum obtained by fitting sine waves by least-squares to the data (Barning, 1963). The unnormalized periodogram for a time series (t_i, y_i) with zero mean ($\bar{y}$=0) is defined as (Lomb, 1976; Scargle, 1982):

$$P(w)=\left\{\frac{[\Sigma_j y_j \cos w(t_j-\tau)]^2}{\Sigma_j \cos^2 w(t_j-\tau)}+\frac{[\Sigma_j y_j \sin w(t_j-\tau)]^2}{\Sigma_j \sin^2 w(t_j-\tau)}\right\} \quad \text{(A1)}$$

where the delay, τ, is defined by,

$$\tan 2w\tau = \frac{\Sigma_j \sin 2wt_j}{\Sigma_j \cos 2wt_j}$$

This power, $P(w)$, is a spectral fitting parameter that displays how closely the data may be fitted with a single harmonic function of frequency w. The larger the value of $P(w)$, the better the fit.

Noisy data produce noisy periodograms. Peaks in a periodogram may therefore not be due to the presence of any real periodic phenomenon at all. They may simply be random fluctuations in periodogram power caused by the presence of a noise component in the data. Peaks arising in this way are spurious: they are not due to any real periodicity. These spurious peaks can be surprisingly large, so it is important to have reliable tests for detecting their presence. Lomb (1976) and Scargle (1982) investigated the statistical behaviour of the periodogram, especially the statistical significance of a signal in the power spectrum. To find an analytic expression for estimations of the significance of the power peaks is important the normalization of the periodogram. There have been some discussions in the literature on how to normalize the periodogram (Scargle, 1982; Horne and Baliunas, 1986; Koen, 1990; Cumming et al., 1999; Hernandez, 1999; Zechmeister and Kürster, 2009). Scargle (1982) normalized the periodogram with the total variance of the data, $P_N(w)=\frac{P(w)}{2\sigma_y}$, but as this variance is normally unknown he replaced it for the sample variance as normalization of the periodogram. This way, the periodogram is a sum of squares of two normally distributed zero-mean variables, and has an exponential probability distribution for random Gaussian noise, independent of the sample pattern.

The likelihood of the existence of a periodic signal can be established with a false alarm probability function (FAP). The FAP, it is to say the probability that no peaks in the power

spectrum have amplitudes greater than z_c for uncorrelated Gaussian noise is:

$$\mathrm{FAP} = 1 - (1 - e^{-z_c})^{n_i} \tag{A2}$$

where n_i is the number of independent frequencies searched.

A power peak is significant with a confidence level greater than P (P=1−FAP) if its power value exceed a critical power level, z_c, given by:

$$z_c = -\mathrm{Ln}\left(1 - (1 - \mathrm{FAP})^{\frac{1}{n_i}}\right) \tag{A3}$$

A2 Examples

In the following we will try, using some examples, to show the main difficulties in the detection of statistical significant signals of a possible planetary wave like atmospheric perturbations in the context of SATI dataset.

The periodogram application to the study of a possible periodic modulations of period close to 2 days is discussed first, in connection with the 1 day regular gaps present in the time series analysed. Later its application to the case of long period signals is discussed, in connection with the length limitation of the time series used (because of the quasi periodic nature of the planetary wave oscillations and the observational characteristic of the dataset).

A2.1 Application to 2 day period signals

The study of 2-day quasi-wave by using night airglow measurements has the additional difficulties related to the regular gaps of 1 day between each night of measurements. The analysis of 2-day wave by using nightly averaged data imposes a lower limit on period detection of 2 days (Nyquist period). So periodic signal present in data of period less than 2 day can not be identified. This problem is solved, partially, by using all the data measured each night. This way signals of short periods can be considered.

To discuss this problem a set of numerical data simulating a periodic signal of 2.6 days of period and amplitude of modulation of 0.1 units has been constructed. A random noise of zero mean and about 0.18 units standard deviation noise has been added to the data. This 2.6 day periodic signal plus noise has been constructed for 5 different time series (see upper panel Fig. A1):

a) 30 days of continuous measurements. The measurements have not gaps from day to day. The measurements are distributed at a rate of 3 data per hour at night and during day.

b) This case is a simulation of 30 days length but measurements are taking only at night. It has regular data periods of 12 h spaced for 1 day gaps.

c) A time series of 30 days total length forming for a night with data followed for a consecutive night without data. The 12 h data periods are regularly spaced by 2 days.

d) A time series of a total length of 15 days (similar to the average length of a time series of one month of data). Nights of data are mixed with some nights of no data simulating irregular gaps (bad weather conditions). In the example there are 12 nights with measurements and 3 nights with no available measurements mixed. The length of the data period during the night has been shorted for some days.

e) A time series with irregular gaps as in the case d) but with a shorter total length, 9 days, with only 6 night of available measurements.

Together these simulations, plotted in the upper panel of Fig. A1, are also plotted the nightly averaged value for each night of data as big solid points.

In the middle panel are plotted the corresponding periodograms obtained for the time series when all the data are used, while in the lower panel are plotted the periodograms calculated for the time series formed with the daily averaged data. The confidence levels of 70% and 95%, calculated with the expression (A3), are shown. The number of independent frequencies is taken as the number of days with available measurements divided by two, considering this the number of natural frequencies of the corresponding time series.

The periodograms are usually calculated at the natural frequencies. Then, if Δt is the average sampling rate, the periodogram should be calculated from the highest possible period, it is the length of the data $N\Delta t$ (lower frequency $w=\frac{1}{N\Delta t}$), to the small possible period, $2\Delta t$ (or Nyquist frequency $w_{Ny}=\frac{1}{2\Delta t}$ higher frequency limit). It is to say at frequencies $\frac{1}{N\Delta t}k$ from k=1 to $N/2$. These are the natural frequencies of the time series. For daily averaged measurements the sampling rate Δt is 1 day and the Nyquist frequency is $0.5\,\mathrm{d}^{-1}$. This imposes a lower limit of 2 days in the detection of a periodic signal. For all the data time series an average sampling rate of 20 min (sampling rate of these simulations) could be used allowing the identification of signals to a lower limit period of 40 min. In the lower panel of Fig. A1 the periodograms have been extended until the period of 1 day for comparison.

For time series simulation of case a) the power peak at 2.6 days is above the level of significance. The spurious peak at 1.6 days is beyond the limit of 2 days for period detection of the time series formed with the daily averaged data. For case b) the results obtained by using nightly averaged data are almost identical to those obtained with averaged data in case a). However when all the data are used (see middle panel) the power of the 1.6 days false peak is smaller than the power of the peak of the true signal at 2.6 days allowing the identification of the signal. For case c) the periodograms show together the peak corresponding to the 2.6 day periodic signal other significant peaks at 1.6, 1.1 and 8.8 days corresponding to false peaks due to the 2 day and 1 day gaps. Although false peaks are weaker when all the data are used (middle panel), these are still strong and may produce false signal identifications. The regular gaps produces very strong

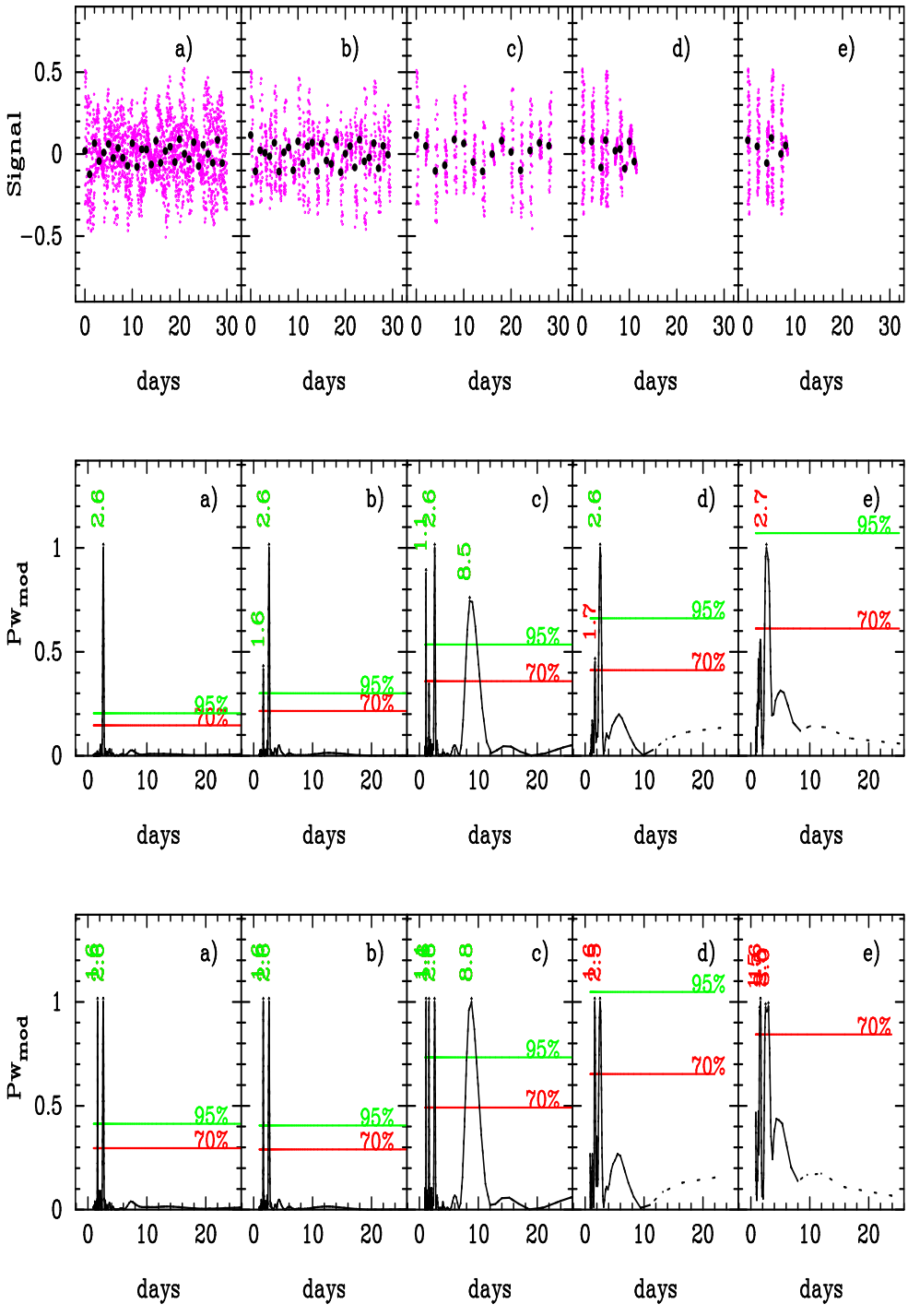

Fig. A1. Upper panel: Numerical simulations of a periodic signal of period 2.6 days plus noise. Points: simulated data at a sampling rate of 3 data per hour. Solid circle: Averaged nightly data. Simulations of 30 days length: **(a)** No gaps **(b)** 1 day gaps. **(c)** 2 day gaps. **(d)** Simulations of 15 day length with gaps of 1 day and irregular 2 day gaps **(e)** as (d) but a simulation of 9 days. Middle panel: Periodograms of all the data time series. Lower panel: Periodograms of nightly averaged data time series.

peaks. Normally, except the observational 1 day gap, the gaps are irregular spaced in the time series, and then the false peaks have small power.

The power of the false peaks at 8.8 and 1.1 days have decreased in case d) because of the lost of regularity in the 2 day gaps but the 1.6 peak corresponding to the 1 day gap

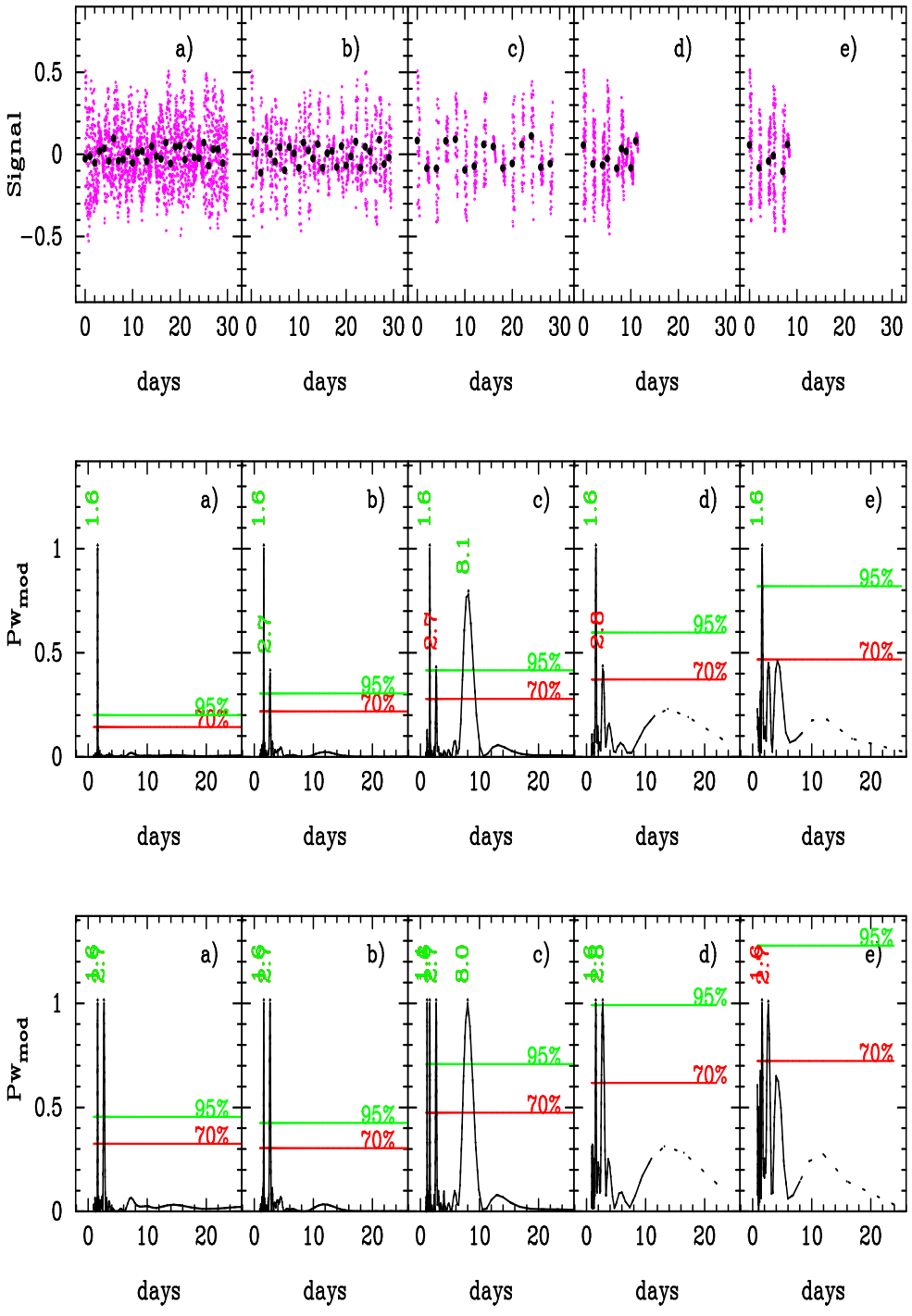

Fig. A2. Upper panel: Simulations of a periodic signal of 1.6 days of period plus noise. Points: data at a rate of 3 data per hours. Solid circle: Averaged nightly data. Simulations: **(a)**, **(b)**, **(c)**, **(d)** and **(e)** as in Fig. A1. Middle panel: Periodograms of all data time series. Lower panel: Periodograms of nightly averaged data time series.

(observational conditions) is still there although with weaker power than the peak at 2.6 days when all the data are used. The short length of the time series in case e) makes the periodograms be noiser and the peaks less significant. But the results are similar to case d).

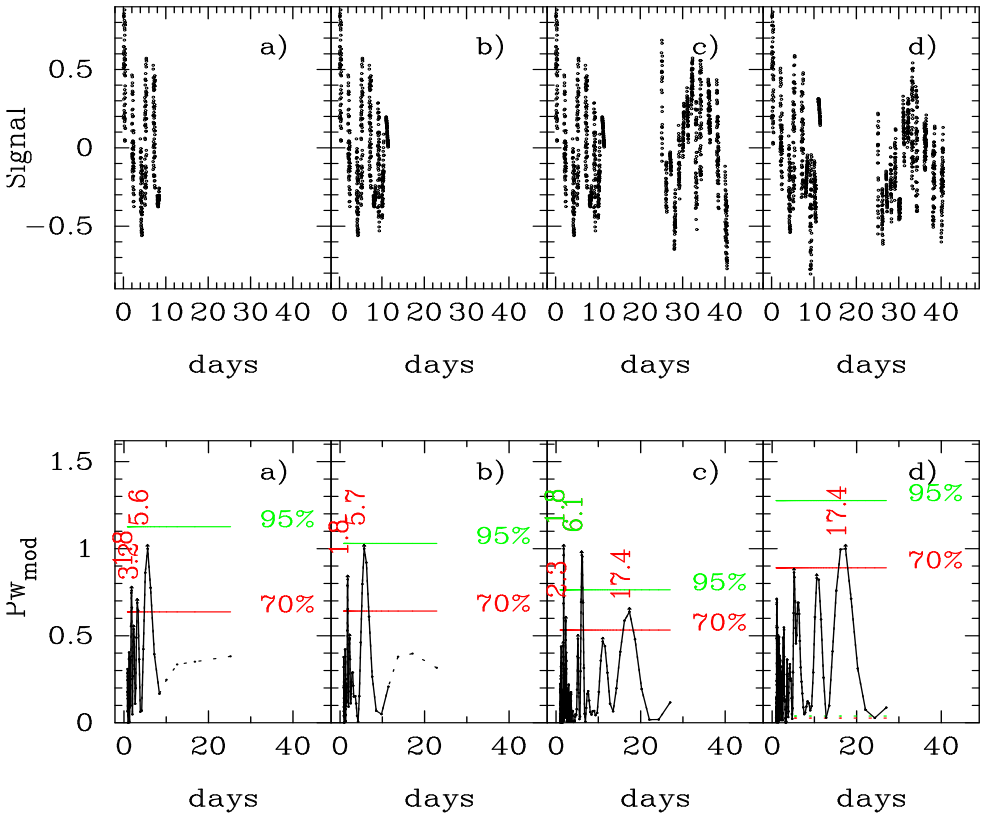

Fig. A3. Upper panel: Simulations of periodic signals of 1.8, 6.2, 11.2 and 16.5 days of periods plus noise. Simulations: **(a)**, **(b)**, **(c)**, and **(d)** see text for details. Lower panel: periodograms.

If we repeat the same simulations but now with a periodic signal of 1.6 day of period, the analysis undertaken with all the data clearly shows the presence of 1.6 day peak as the strongest peak while the nightly averaged data should indicate a peak at 2.6 day period clearly present in the data (see Fig. A2 for comparison).

As conclusion, although the periodograms obtained by using all the data do not avoid the presence of false peaks due to the 1 day gap of the dataset, it may reduce the value of the power of the false peaks in some degree, allowing the better identification of a possible real signal of periods around 2 days present in the data. The better the time series is, the better the peaks of the true signals will be defined in the periodogram and the false peaks will be reduced.

A2.2 Application to long period signals

The limited length of the time series because of the quasi wave nature of the planetary wave type oscillations make also difficult the study of such long period signals. The limited length produces very wide peaks in the periodogram making very difficult the identification of individual signals.

We have simulated four periodic signals of periods of 1.8, 6.2, 11.2 and 16.5 days, respectively, and amplitudes of 0.2 units for the shorter period signals (2.2 and 6.2 day) and 0.1 units for the longer period signals (11.2 and 16.5 days) plus a random noise of about 0.30 units of standard deviation noise. These signals have been simulated for the following cases (see Fig. A3): a) a time series of total length of 9 days with 6 nights of measurements mixed with 3 nights without measurements; b) a time series of total length of 16 days, 12 nights with measurements mixed with 4 nights of no available data; c) a time series of 40 days formed by a first set of 16 days length (as the case b)) plus a gap of 14 days of no available measurements followed by other set of 12 days length (3 of them with no available measurements), and d) the same that case c), but, here, the periods of the four signals are allowed to have random fluctuations in the periods (these random fluctuations in the periods have variances close to 0.12 days).

For case a) only periodic signals of periods smaller than 9 days (the temporal length of the data 9 days) can be inferred. Power peaks at periods of 1.8 and 5.6 days above a 70% confidence level can be seen. A false peak at 3.2 days is also present above these confidence level. When the total length of the data increase to 16 days (case b)) the peaks corresponding to the periodic signals at around 2 and 6 days are more significant. For larger time series (case c)) the four

peaks of the corresponding four signals are present but the confidence level is slightly smaller than 70% for the 11 day signal, although is larger than 95% for the 2 day and 6 day signals. So, even although the 11 day signal is in the data its level of statistical significance is less than 70% and should not be identified if a limit in the confidence level of 70% was required as selection criterion for the statistical significant peaks.

The presence of many modulations of long periods can also mask other closer peaks at shorter period: first by the wide shape of the peaks which may mask other closer peaks and second, by increasing the noise level of the periodogram and then making difficult the detection of other possible signals. Longer temporal time series allow to increase the temporal or frequency resolution in the periodograms allowing the detection of signals of long periods that could not be spectral separated in short length time series. However, the modulations that we are studying are quasi periodic (small period fluctuations are present). These fluctuations produces additional noise and may hide the periodic modulations preventing the detection. Case d) shows how a small period fluctuation can affect the data. In this example the power peaks corresponding to modulations of shorter periods (those corresponding to the 2 and 6 days of periods) have decreased. The number of noisy peaks in the periodogram in the region of shorter periods have increased. Only the power of the peak at 16 days is maintained above a confidence level of 70%.

It is seem intuitive to think that fluctuations will affect to signals of short periods stronger than to those of long periods. Then the detection of the short period signals will be more difficult in long time series. A compromise between the level of confidence and the length of the time series has to be chosen.

Acknowledgements. This research was partially supported by the Spanish MICINN under projects AYA2006-06375 and AYA2008-03498/ESP, EC FEDER funds and the Junta de Andalucía. We very gratefully acknowledge the staff of Sierra Nevada Observatory for their help and assistance with the SATI instrument. We wish to thank the referees and the topical Editor Christoph Jacobi for useful comments and suggestions.

Topical Editor C. Jacobi thanks F. Mulligan and R. Lowe for their help in evaluating this paper.

References

Altadill, D. and Apostolov, E. M.: Time and scale size of planetary wave signatures in the ionospheric F region: Role of the geomagnetic activity and mesosphere/lower thermosphere winds, J. Geophys. Res., 108, 1403, doi:10.1029/2003JA010015, 2003.

Baker, D. J. and Stair Jr., A. T.: Rocket measurements of the altitude distribution of hydroxyl airglow, Phys. Scripta, 37, 611–622, 1988.

Barning, F. J. M.: The numerical analysis of the light-curve of 12 Lacertae, B. Astr. Inst. Netherlands, 17, 22, 1963.

Buriti, R. A., Takahashi, H., Lima, L. M., and Medeiros, A. F.: Equatorial planetary waves in the mesosphere observed by airglow periodic oscillations, Adv. Space Res., 35, 2031–2036, 2005.

Chshyolkova, T., Manson, A. H., and Meek, C. E.: Climatology of the quasi two-day wave over Saskatoon (52° N, 107° W): 14 Years of MF radar observations, Adv. Space Res., 35, 2011–2016, 2005.

Cumming, A., Marcy, G. W., and Butler, R. P.: The Lick Planet Search: Detectability and Mass Thresholds, The Astrophys. J., 526, 890–915, 1999.

Espy, P. J., Stegman, J., and Witt, G.: Interannual variations of the quasi-16-day oscillation in the polar summer mesospheric temperature, J. Geophys. Res., 102, 1983–1990, 1997.

Forbes, J. M. and Groves, G. V.: Atmospheric tides below 80 km, Adv. Space Res., 10, 119–125, 1990.

Forbes, J. M., Hagan, M. E., Miyahara, S., Vial, F., Manson, A. H., Meek, C. E., and Portnyagin, Y. I.: Quasi 16-day oscillation in the mesosphere and lower thermosphere, J. Geophys. Res., 100, 9149–9164, 1995.

Greer, R. G. H., Murtagh, D. P., McDade, I. C., Dickinson, P. H. G., Thomas, L., Jenkins, D. B., Stegman, J., Llewellyn, E. J., Witt, G., Mackinnon, D. J., and Williams, E. R.: Eton 1: A date base pertinent to the study of energy transfer in the oxygen nightglow, Planet. Space Sci., 34, 771–788, 1986.

Hernandez, G.: Time series, periodograms, and significance, J. Geophys. Res., 104, 10355–10368, 1999.

Hirota, I. and Hirooka, T.: Normal mode Rossby waves observed in the upper stratosphere. I – First symmetric modes of zonal wavenumbers 1 and 2, J. Atmos. Sci., 41, 1253–1267, 1984.

Hirooka, T.: Normal Mode Rossby Waves as related by UARS/ISAMS Observations, J. Atmos. Sci., 47, 1277–1285, 2000.

Hocke, K.: Phase estimation with the Lomb-Scargle periodogram method, Ann. Geophys., 16, 356–358, 1998.

Holton, J.: An introduction to dynamic meteorology, Ed. Academic Press, 320, 1972.

Horne, J. H. and Baliunas, S. L.: A prescription for period analysis of unevenly sampled time series, Astrophys. J., 302, 757–763, 1986.

Jacobi, C., Schminder, R., and Krschner, D.: Non-linear interaction of the quasi 2-day wave and long-term oscillations in the summer midlatitude mesopause region as seen from LF D1 wind measurements over Central Europe (Collm, 52° N, 15° E), J. Atmos. Solar-Terr. Phys., 60, 1175–1175, 1998.

Jacobi, Ch., Hoffmann, P., and Kürschner, D.: Trends in MLT region winds and planetary waves, Collm (52° N, 15° E), Ann. Geophys., 26, 1221–1232, 2008, http://www.ann-geophys.net/26/1221/2008/.

Jiang, G.-Y., Xiong, J.-G., Wan, W.-X., Ning, B.-Q., Liu, L.-B., Vincent, R. A., and Reid, I.: The 16-day waves in the mesosphere and lower thermosphere over Wuhan (30.6° N, 114.5° E) and Adelaide (35° S, 138° E), Adv. Space Res., 35, 2005–2010, 2005.

Koen, Ch.: Significance testing of periodogram ordinates, Astrophys. J., 348, 700–702, 1990.

Lastovicka, J.: Observations of tides and planetary waves in the atmosphere-ionosphere system, Adv. Space Res., 20, 1209–1222, 1997.

Laštovička, J., Križan, P., Šauli, P., and Novotná, D.: Persistence of the planetary wave type oscillations in *f*oF2 over Europe, Ann. Geophys., 21, 1543–1552, 2003, http://www.ann-geophys.net/21/1543/2003/.

Lawrence, A. R. and Jarvis, M. J.: Initial comparisons of planetary waves in the stratosphere, mesosphere and ionosphere over Antarctica, Geophys. Res. Lett., 28, 203–206, 2001.

Liu, G. and Shepherd, G. G.: Perturbed profiles of oxygen nightglow emissions as observed by WINDII on UARS, J. Atmos. Solar-Terr. Phys., 68, 1018–1028, 2006a.

Liu, G. and Shepherd, G. G.: An empirical model for the altitude of the OH nightglow emission, Geophys. Res. Lett., 33, L09805, doi:10.1029/2005GL025297, 2006b.

Lomb, N. R.: Least-squares frequency analysis of unequally spaced data, Astrophys. Space Sci., 39, 447–462, 1976.

López-González, M. J., Rodríguez, E., Wiens, R. H., Shepherd, G. G., Sargoytchev, S., Brown, S., Shepherd, M. G., Aushev, V. M., López-Moreno, J. J., Rodrigo, R., and Cho, Y.-M.: Seasonal variations of O_2 atmospheric and OH(6-2) airglowand temperature at mid-latitudes from SATI observations, Ann. Geophys., 22, 819–828, 2004, http://www.ann-geophys.net/22/819/2004/.

López-González, M. J., Rodríguez, E., Shepherd, G. G., Sargoytchev, S., Shepherd, M. G., Aushev, V. M., Brown, S., García-Comas, M., and Wiens, R. H.: Tidal variations of O_2 Atmospheric and OH(6-2) airglow and temperature at mid-latitudes from SATI observations, Ann. Geophys., 23, 3579–3590, 2005, http://www.ann-geophys.net/23/3579/2005/.

López-González, M. J., Rodríguez, E., Shepherd, G. G., Shepherd, M. G., Sargoytchev, S., Aushev, V. M., García-Comas, M., Brown, S., and Wiens, R. H.: Atmospheric band and OH(6-2) airglow and temperature variability over Spain using SATI observations: Planetary scale oscillations during autumn, Can. J. Phys., 85, 153–172, 2007.

Luo, Y., Manson, A. H., Meek, C. E., Meyer, C. K., and Forbes, J. M.: The quasi 16-day oscillations in the mesosphere and lower thermosphere at Saskatoon (52° N, 107° W), 1980–1996, J. Geophys. Res., 105, 2125–2138, 2000.

Luo, Y., Manson, A. H., Meek, C. E., Meyer, C. K., Burrage, M. D., Fritts, D. C., Hall, C. M., Hocking, W. K., MacDougall, J., Riggin, D. M., and Vincent, R. A.: The 16-day planetary waves: multi-MF radar observations from the arctic to equator and comparisons with the HRDI measurements and the GSWM modelling results, Ann. Geophys., 20, 691–709, 2002, http://www.ann-geophys.net/20/691/2002/.

Manson, A. H., Meek, C. E., Chshyolkova, T., Avery, S. K., Thorsen, D., MacDougall, J. W., Hocking, W., Murayama, Y., Igarashi, K., Namboothiri, S. P., and Kishore, P.: Longitudinal and latitudinal variations in dynamic characteristics of the MLT (70–95 km): a study involving the CUJO network, Ann. Geophys., 22, 347–365, 2004, http://www.ann-geophys.net/22/347/2004/.

Manson, A. H., Meek, C. E., Chshyolkova, T., Avery, S. K., Thorsen, D., MacDougall, J. W., Hocking, W., Murayama, Y., and Igarashi, K.: Wave activity (planetary, tidal) throughout the middle atmosphere (20–100 km) over the CUJO network: Satellite (TOMS) and Medium Frequency (MF) radar observations, Ann. Geophys., 23, 305–323, 2005, http://www.ann-geophys.net/23/305/2005/.

Meek, C. E., Manson, A. H., Franke, S. J., Singer, W., Hoffmann, P., Clark, R. R., Tsuda, T., Nakamura, T., Tsutsumi, M., Hagan, M., Fritts, D. C., Isler, J., and Portnyagin, Y. I.: Global study of northern hemisphere quasi-2-day wave events in recent summers near 90 km altitude, J. Atmos. Terr. Phys., 58, 1401–1411, 1996.

Mitchell, N. J., Middleton, H. R., Beard, A. G., Williams, P. J. S., and Muller, H. G.: The 16-day planetary wave in the mesosphere and lower thermosphere, Ann. Geophys., 17, 1447–1456, 1999, http://www.ann-geophys.net/17/1447/1999/.

Murphy, D. J., French, W. J. R., and Vincent, R. A.: Long-period planetary waves in the mesosphere and lower thermosphere above Davis, Antarctica, J. Atmos. Solar-Terr. Phys., 69, 2118–2138, 2007.

Namboothiri, S. P., Kishore, P., and Igarashi, K.: Climatological studies of the quasi 16-day oscillations in the mesosphere and lower thermosphere at Yamagawa (31.2° N, 130.6° E), Japan, Ann. Geophys., 20, 1239–1246, 2002, http://www.ann-geophys.net/20/1239/2002/.

Nozawa, S., Brekke, A., Maeda, S., Aso, T., Hall, C. M., Ogawa, Y., Buchert, S. C., Röttger, J., Richmond, A. D., Roble, R., and Fujii, R.: Mean winds, tides, and quasi-2 day wave in the polar lower thermosphere observed in European Incoherent Scatter (EISCAT) 8 day run data in November 2003, J. Geophys. Res., 110, A12309, doi:10.1029/2005JA011128, 2005.

Pancheva, D., Anufriev, A., and Lastovicka, J.: Planetary wave activity in the lower ionosphere during the DYANA campaign, J. Atmos. Solar-Terr. Phys., 56, 1963–1968, 1994.

Pancheva, D. V., Mukhtarov, P. J., Shepherd, M. G., Mitchell, N. J., Fritts, D. C., Riggin, D. M., Franke, S. J., Batista, P. P., Abdu, M. A., Batista, I. S., Clemesha, B. R., and Kikuchi, T.: Two-day wave coupling of the low-latitude atmosphere-ionosphere system, J. Geophys. Res., 111, A07313, doi:10.1029/2005JA011562, 2006.

Riggin, D. M., Liu, H.-L., Lieberman, R. S., Roble, R. G., Russell, J. M., Mertens, C. J., Mlynczak, M. G., Pancheva, D., Frank, S. J., Murayama, Y., Manson, A. H., Meek, C. E., and Vincent, R. A.: Observations of the 5-day wave in the mesosphere and lower thermosphere, J. Atmos. Solar-Terr. Phys., 68, 323–339, 2006.

Salby, M. L.: Rossby Normal Modes in Nonuniform Background Configurations. Part II. Equinox and Solstice Conditions, J. Atmos. Sci., 38, 1827–1840, 1981.

Sargoytchev, S., Brown, S., Solheim, B. H., Cho, Y.-M., Shepherd, G. G., and López-González, M. J.: Spectral airglow temperature imager (SATI) – a ground based instrument for temperature monitoring of the mesosphere region, Appl. Optics, 43, 5712–5721, 2004.

Scargle, J. D.: Studies in astronomical time series analysis. II – Statistical aspects of spectral analysis of unevenly spaced data, Astrophys. J., 263, 835–853, 1982.

Sivjee, G. G., Walterscheid, R. L., and McEwen, D. J.: Planetary wave disturbances in the Arctic winter mesopause over Eureka (80° N), Planet. Space Sci., 42, 973–986, 1994.

Takahashi, H., Buriti, R. A., Gobbi, D., and Batista, P. P.: Equatorial planetary wave signatures observed in mesospheric airglow emissions, J. Atmos. Solar-Terr. Phys., 64, 1263–1272, 2002.

Thayaparan, T., Hocking, W. K., and MacDougall, J.: Amplitude, phase, and period variations of the quasi 2-day wave in the mesosphere and lower thermosphere over London, Canada (43° N, 81° W), during 1993 and 1994, J. Geophys. Res., 102, 9461–9478, 1997.

Vincent, R. A.: Planetary and gravity waves in the mesosphere and lower thermosphere, Adv. Space Res., 10, 93–101, 1990.

Wiens, R. H., Moise, A., Brown, S., Sargoytchev, S., Peterson, R. N., Shepherd, G. G., López-González, M. J., López-Moreno, J. J., and Rodrigo, R.: SATI: A Spectral Airglow Temperature Imager, Adv. Space Res., 19, 677–680, 1997.

Williams, C. R. and Avery, S. K.: Analysis of long-period waves using the mesosphere-stratosphere-troposphere radar at Poker Flat, Alaska, J. Geophys. Res., 97, 20855–20861, 1992.

Witt, G., Stegman, J., Solheim, B. H., and Llewellyn, E. J.: A measurement of the $O_2(b^1\Sigma_g^+ - X^3\Sigma_g^-)$ atmospheric band and the OI(^{1}S) green line in the nightglow, Planet. Space Sci., 27, 341–350, 1979.

Witt, G., Stegman, J., Murtagh, D. P., McDade, I. C., Greer, R. G. H., Dickinson, P. H. G., and Jenkins, D. B.: Collisional energy transfer and the excitation of $O_2(b^1\Sigma_g^+)$ in the atmosphere, J. Photochem., 25, 365–378, 1984.

Wu, D. L., Hays, P. B., and Skinner, W. R.: Observations of the 5-day wave in the mesosphere and lower thermosphere, Geophys. Res. Lett., 21, 2733–2736, 1994.

Xiong, J., Wan, W., Ning, B., Liu, L., and Gao, Y.: Planetary wave-type oscillations in the ionosphere and their relationship to mesospheric/lower thermospheric and geomagnetic disturbances at Wuhan (30.6° N, 114.5° E), J. Atmos. Solar-Terr. Phys., 68, 498–508, 2006.

Yee, J.-H., Talaat, E. R., and Zhu, X.: 6.5 Day planetary waves in the mesosphere and lower thermosphere, Adv. Space Res., 27, 1761–1765, 2001.

Zechmeister, M. and Kürster, M.: The generalised Lomb-Scargle periodogram. A new formalism for the floating-mean and Keplerian periodograms, Astron. Astrophys., 496, 577–584, 2009.